International Journal of Automotive Technology, Vol. 3, No. 4, pp. 137–145 (2002)

1229-9138/2002/004-02

A STUDY ON EXPERIMENTAL CHARACTERISTICS OF ENERGY ABSORPTION CONTROL IN THIN-WALLED TUBES FOR THE USE OF VEHICULAR-STRUCTURE MEMBERS

S.-K. KIM[1)*], K.-H. IM[2)], C.-S. HWANG[3)] and I.-Y. YANG[4)]

[1)]Department of Automobile Engineering, Iksan National College, Chonbuk 570-752, Korea
[2)]Department of Automotive Engineering, Woosuk University, Chonbuk 565-701, Korea
[3)]Department of Mechanical Design Engineering Graduate School of Chosun University, Kwangju 501-759, Korea
[4)]School of Mechanical Engineering, Chosun University, Kwangju 501-759, Korea

(Received 22 April 2002; Revised 3 August 2002)

ABSTRACT–Automobiles should be designed to meet the requirements and standards for the protections of passengers in a car accident. One of safety factors is an absorbing capacity in collision. Many vehicles have been designed based on the criterion of the absorbing capacity. Therefore a controller has been developed in order to control and increase the absorbing capacity of impact energy in automobile collision. The capacity of impact energy will be improved regardless of vehicular-structure members and shapes. An air-pressure horizontal impact tester for crushing has been built up for the evaluation of energy absorbing characteristics in collision. Influence of height, thickness and clearance in the controller have been considered to predict and control the energy absorbing capacity. Aluminum alloy (Al) tubes (30, 39, 44 mm in inner dia. and 0.8, 1.0, 1.2 mm in thickness) are tested by axial loading. The energy absorbing capacity of Al tubes have been estimated in cases of with-controller and without-controller, respectively based on height, thickness, clearance of an controller.

KEY WORDS : Energy absorption, Absorbing capacity, Controller of energy absorption and impact loading

1. INTRODUCTION

The object of vehicular design is to understand general performance to satisfy the standards and the requirements; calmness, the feelings of stability, firm handling and pleasantness. The safety capacity which means to keep the safety of passengers up in a car accident should be affected by the conditions of collision, the structural integrity and protective equipment for passengers. Head-end collisions including inclined collision amount to about 70 percent of accidents compared to those occurring on the side or rear collisions. Thus, attention to safety capacity has increasingly been focused on head-end collisions in recent years (Ishikawa, 1985 and Haug *et al.*, 1996).

Actually a head-on frame structure of vehicles is supporting the engine and suspension systems, and playing an important role of containing other attachments in position. Above all things, the structures of vehicles must absorb the impact energy especially in a head-on collision (Pritz, 1983 and Kevin, 1986). If the head-on frame structure enough absorbs the impact energy in a head-on accidents, the collision burden of structural frames enclosing the car body could be reduced down and also the safety of passenger could be kept up efficiently. This means that the head-end structure is the most important factor in the characteristics of front-head collision. So we need to consider the characteristics of energy absorption and the collapse by plastic deformation on a simple structure which endures a massive collision before predicting forehead collision capacity (Mahmood *et al.*, 1981, Li *et al.*, 1990 and Singace, 1999).

Previous studies on the collapse characteristics of thin-walled structural members have been performed to analyze the mean collapse loading based on experimental and numerical analyses. Particularly, front-side members of cars play an important role on the energy absorption when cars come into head-on collision. Also, vehicles for passengers are consisted of many thin-walled members like a thin tube and a box to decrease the weight. The box shapes of thin-walled structures are spot usually welded. Also the impact energy absorption abilities have been studied based on the crushing behavior, and the folding-formation mechanism have been investigated assuming

*Corresponding author. e-mail: skyu@iksan.ac.kr

that a compact-mode folding is generated when members are crushed. White, Wierzbicki and Henry have studied the energy absorption abilities by solving mean-crushing loading based on axisymmetric and non-axisymmetric modes during the crushing process (White *et al.*, 1999 and 1999, Wierzbicki *et al.*, 1983 and Henry, 1985). Also, the crushing characteristics have been reviewed with the variation of width ratio of thin-walled members and welding distance (Cha *et al.*, 2001).

In the present paper, an air-pressured horizontal impact testing machine has been constructed newly for crushing and measuring the impact load and a deformation. The crushing tests of thin-walled circular tubes are carried out to investigate the energy absorption abilities. In particular, energy absorption abilities of side members could be higher than any other parts in a front collision. Also, a controller has been developed in order to increase the energy absorption abilities under the same conditions of specimens. The results from with-controller impact tests are compared with those from without-controller impact tests and the difference has been discussed. The effects of the height, thickness, clearance and materials of the specimen on crushing behaviors are studied. This paper focuses on improving energy absorption abilities in crushing by using a controller.

2. SPECIMENS AND CONTROLLER

2.1. Specimen Configurations

As the specimen, the circular tubes are made of aluminum alloy (Al 6063) which was machined to thin-walled members. At that time, a lathe is used to machine the specimens with using a solid drawn pipe in order to keep away with torsion of specimens. The axial length is fixed in 200 mm, of which the length does not have the Euler's buckling. Also, the length has not been affected by a controller's height in crushing absorption process and also has been suitable for reproducibility. Detailed dimensions and symbols of the Al tubes are shown in Table 1. The end edge of specimens is cut at the angle of 30° to generate easily the initial deformation on the edge.

2.2. Controller Setup

Improvement of energy absorption abilities has been required in order to keep the safety of passenger up with using the structural members of vehicles. So, a controller is developed to increase the absorption energy in collision. As shown in Figure 1, D means 31.6 mm, 32 mm, 32.4 mm, 33 mm, 40.6 mm, 41 mm, 41.4 mm, 42 mm, 45.6 mm, 46 mm, 46.4 mm and 48 mm. A controller is machined in consideration of diameter and clearance of specimens shown in Table 1, h means 5 mm, 10 mm and 20 mm, and t does 14 mm and 20 mm respectively.

3. CRUSHING EXPERIMENTATION

3.1. Static Crushing Tests

Static crushing experimentation has been made using the universal testing machine (UTM, Instron 8801). Axial compression is loaded on the tube with 200 mm in length till the final displacement of specimens comes to 90 mm. Namely, the collapse tests are made to the deformation length, 110 mm of the specimens. The UTM was utilized with the compression rate of 10 mm/min. in order to remove effects of strain rate. Lubricating oil is used to keep the contact between specimen and pressurized plate

Table 1. Definition of the specimen number.

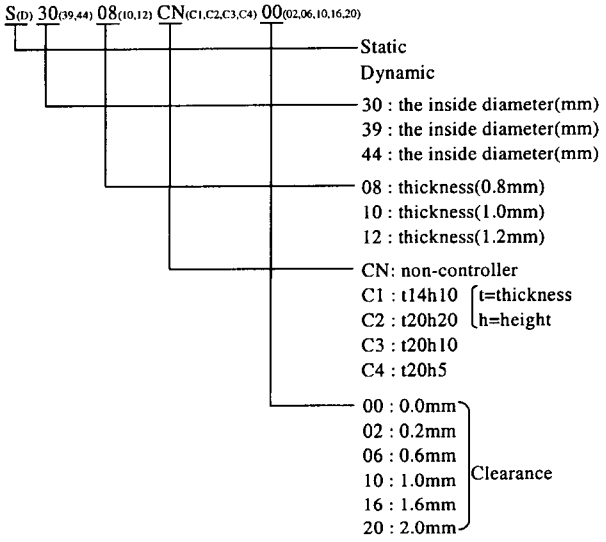

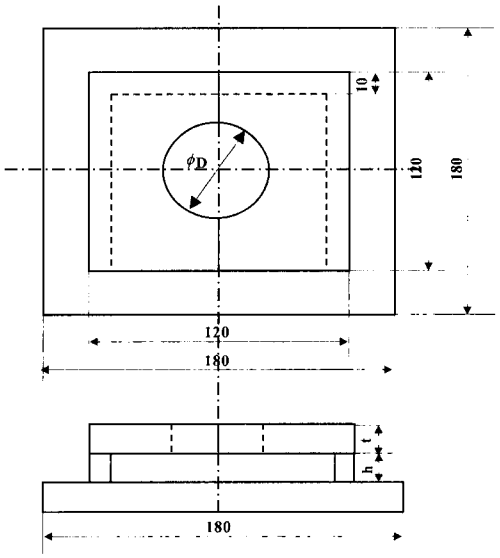

Figure 1. Controller of energy absorption.

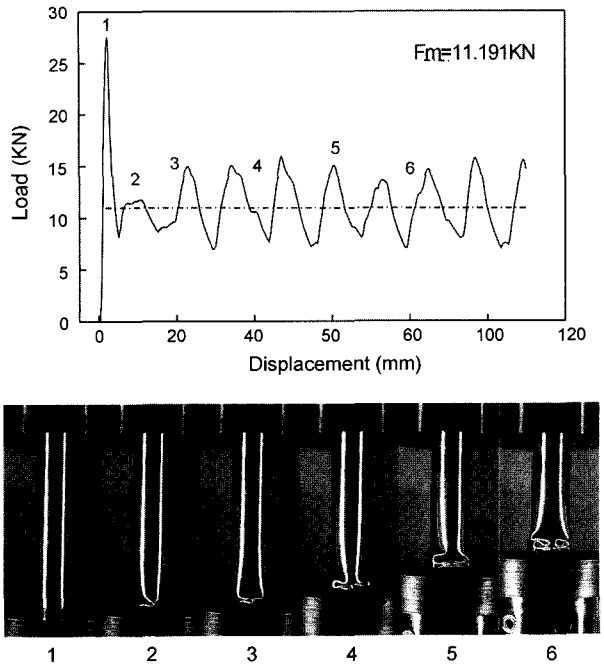

Figure 2. Load-displacement curve and collapsed process of specimen, S4410CN.

to be smooth. Also, after inserting a controller between specimen and pressurized plates, influences of height, thickness and clearance in the controller have been

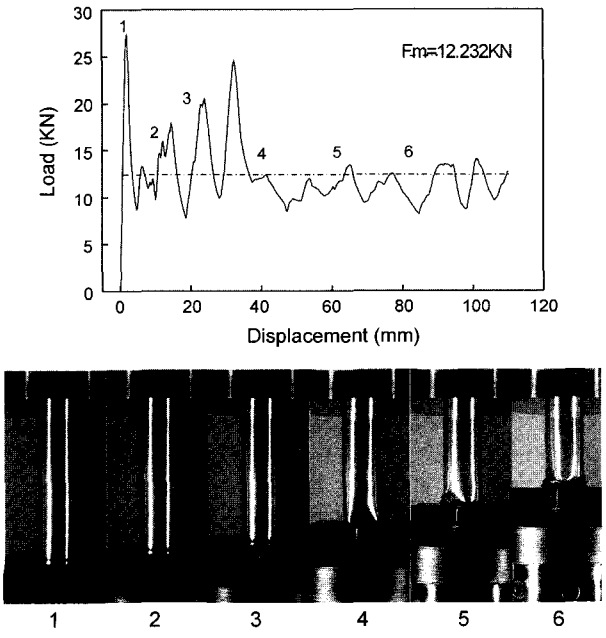

Figure 3. Load-displacement curve and collapsed process of sepcimen, S4410C300.

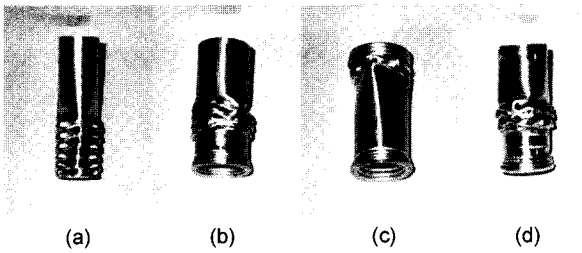

Figure 4. Shape of collapsed specimens (a: S3010CN, b: S4408C100, c: S4412C100 and d: S4412C300).

considered. Load-displacement curve could be obtained by the displacement control in crushing process. The absorption energy volume could be considered as an area of load-displacement curve in collision tests. The energy absorbed E_a is obtained by integrating the crush loads over the stable crush region of the load-displacement curve. The crush load F, is calculated with the absorbed energy divided by the deformed length.

$$E_a=\int_{L_0}^{L} F\,dl \tag{1}$$

Figures 2 and 3 show the crushing process and load-displacement curve of static collapse experimentation in case of with- and without-controller, respectively when specimens, which have 44 mm inside diameter and 10 mm in thickness, are compressed at a rate of 10 mm/min. No. 1 means 0 mm in collapsed displacement, No. 2 does 10 mm, No. 3 does 20 mm, No. 4 does 40 mm, No. 5 does 60 mm, and No. 6 does 80 mm as shown in Figures 2 and 3. Numbers in figures and photos below are agreed with each other. Figures 4 and 6 show shapes after the static collapse experimentation.

3.2. Crushing Tests

Impact collapsed tests are carried out to measure deformation and loading during the crushing process as shown in the static collapsed experimentation. Crushing displacement of specimens is assumed as a moving distance of input impactor. At that time displacements of input impactor were measured by using non-contacting optical displacement measurement system (Zimmer 100F) which catches up displacement of cross head. Also, loads of specimens can be obtained based on variations of strain gages from loadcell fixed at input and output impactor. The velocity of input impactor was measured just before collision on the specimen by determining the time taken for it to pass two fine laser beams located a known distance apart. Here, the impact kinetic energy should be equal to the kinetic energy of input impactor. The energy was 1600J (with a velocity of 6.10 m/s) and 1982J (with a velocity of 6.79 m/s). An input impactor weight is 86 kg and the range of impact

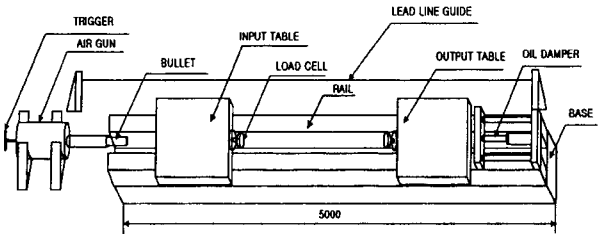

Figure 5. Horizontal impact testing setup for crushing.

velocities covers from 6.10 m/s to 6.79 m/s under air pressures on a compressor (0.7 Mpa). The load-deformation curves can be evaluated from curves of the load and the deformation cancelling the time out. The characteristics of members are estimated with the absorbed energy (E_a), total absorbed energy (E_t), mean collapsed loads (F_m) and maximum collsped loads ($F_{max.}$). In particular even if the impact energy is the same the constant absorbed energy can not quantitatively be evaluated due to the different length of collapses under the same impact energy. Therefore, to quantitatively confirm the absorbed energy in the static and impact collapse experimentation, total length, 200 mm in all specimens has been assumed to be collapsed. The total absorbed energy (E_t) equation is as follows (Kim *et al.*, 2001);

$$E_t=E_a\bar{J} \tag{2}$$

where $\bar{J}$ ($=L/S$) is a reversed stroke efficiency. Here S is a deformed distance of specimens and L is 200 mm prior to deformation. The impact testing machine of an air-pressured horizontality designed and produced specially for the present research provides the steel crosshead to move on and crush a specimen on the load cell, as shown in Figures 5. Figure 6 shows shapes of after-impact collapse experimentation.

3.4. Measurement System

The curves of the load and the deformation during crushing of the specimens are estimated in the impact

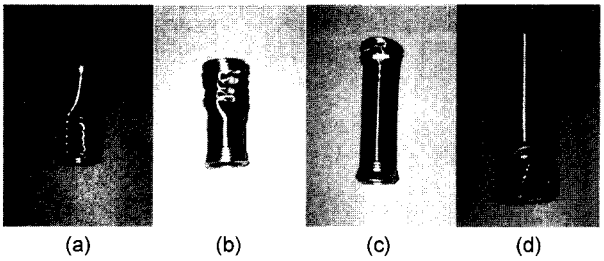

Figure 6. Shape of collapsed specimens (a: D3008CN, b: D3008C300, c: D3010C100 and d: D4408C204).

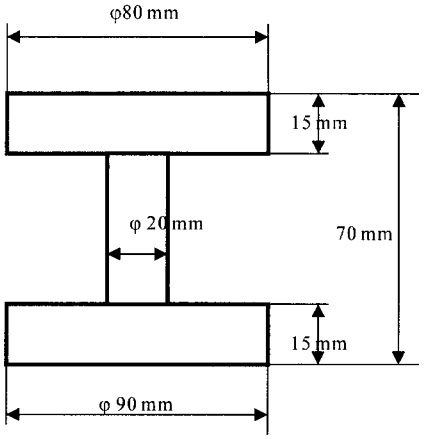

Figure 7. Dimension of load cell.

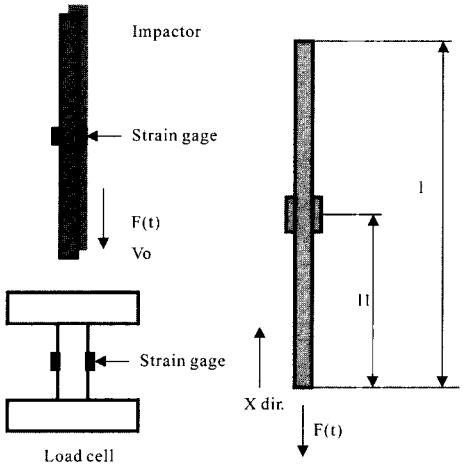

Figure 8. Calibration for load cell.

collapsed experimentation. The load curve is measured by the home-made load cell. The load cell on the bottom of the machine was machined from soild cylinder of mild steel as shown in Figure 7. This consists of three elements: two flanges and a straight bar. At the middle point of the straight bar, a pair of semi-conductor strain gages are bonded symmetrically about the center axis. These gages are connected in series to cancel the bending moment component. The load curve is estimated multiplying the strain curve by sectional are and Young's modulus of straight bar location. In order to confirm the dynamic characteristics of the load cell, the impact bar was performed as shown in Figure 8. The impactor which length is 400 mm and diameter is 10 mm was collided with the top of flange of the load cell. At the case, load curve $F(t)$ is computed from the strain curve $\varepsilon(t)$ at the middle point of the impactor according to the following equation (3) as follows:

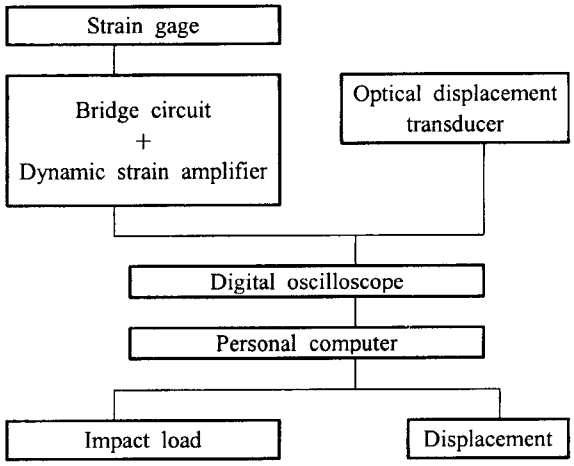

Figure 9. Diagram of measurement system.

$$F(t)=AE\varepsilon\left(t+\frac{l}{2K}\right)\cdot H\left(t+\frac{l}{2K}\right)$$
$$\varepsilon\left(t+\frac{l}{2K}\right)\cdot H\left(t+\frac{l}{2K}\right),\quad K^2=\frac{\rho}{E} \tag{3}$$

where $H(t)$ is step function. And A, E, l, ρ and t mean the sectional area, Young's modulus, the length, the density of the impactor and the time, respectively. Also, the impact load $f(t)$ was measured by the load cell. By the FFT procedure for $F(t)$ and $f(t)$, the frequency responses $F(\omega)$ and $f(\omega)$ with frequency ω were estimated. $f(\omega)$ can be treated as the reference value as shown in equation (3). $F(\omega)$ is normalized by $f(\omega)$ to estimate the dynamic characteristics of the load cell. As the results, $f(\omega)/F(\omega) \fallingdotseq 1$ till approximately 3 kHz which is valid in this experimentation. Therefore the low-pass-filter of approximately 3 kHz is applied to the load curve. The deformation curve of the specimen was measured by the optical displacement transducer (Zimmer, 100F) which had high dynamic response. The deformation at the top of the specimen coincides with the motion of the crosshead during crushing as the crosshead is much more rigid than the specimen. The displacement of crosshead was measured by the optical displacement transducer in order to estimate the deformation of tubes. The impact velocity just before crushing was taken by using two laser beams. Figure 9 shows the measurement system. The strain gage signal from the load cell, and the output of the optical displacement transducer are memorized into the transient digital analyzer. The sampled data in the analyzer are transferred to the personal computer, and converted to the curve of load and deformation, respectively. The load-deformation curves could be estimated cancelling the time out. So the characteristics from the load-deformation curves have been evaluated with the absorbed energy

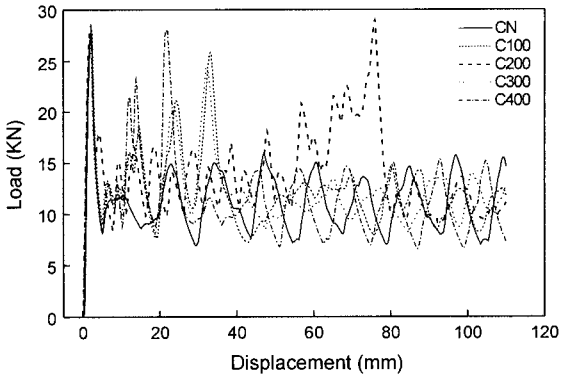

Figure 10. Static load-displacement characteristics for the circular tube, S4410.

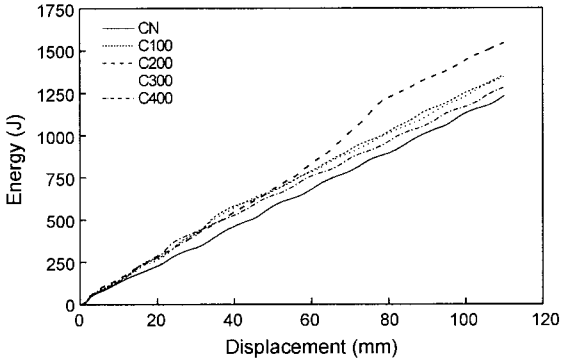

Figure 11. Static energy-displacement characteristics for the circular tube, S4410.

obtained from the crushing length and the mean stress.

4. RESULTS AND DISCUSSION

After an initial deformation of specimens had started at a 30°-machined trigger on one-side tube edge, the progressive crushing modes were mostly observed under the static collapse tests. And in the dynamic collapse test, the initial deformation was generated at the direction of a 30°-machined trigger; however in addition the deformation was generated at the opposite direction of a 30°-machined trigger. Tables 2 and 3 show results of energy absorption abilities under static and dynamic loading, respectively. Figures 10, 11, 12 and 13 show the load-displacement diagram and absorption energy-displacement diagram obtained from the static collapse tests. In the case of non-controller collapse tests, axisymmetric, non-axisymmetric and mixed modes were observed as shown by previous workers. When the specimens are collapsed, the regular modes are not easily observed only if a moving point of plastic hinge has a slightly different distance in crushing process as the controller used in this study is holding an

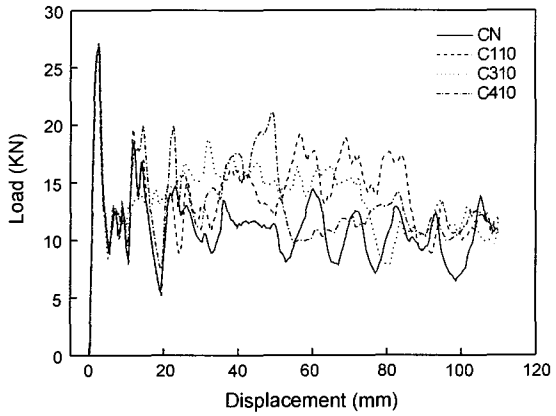

Figure 12. Static load-displacement characteristics for the circular tube, S3910.

arbitrary location of specimens. Figure 10 shows a static load-displacement diagram for the circular tube with inner diameter, 44 mm and 1.0 mm in thickness, and the second peak has been observed in the Figure 10 with the exception of CN specimen. The second peak value is similar to that of the first peak. Also, Figure 11 shows a linear increasing of a static energy-displacement diagram based on the effects of a controller. The effects of controller's thickness do not influence the relation of energy and displacement for the specimens. Also, in the case of specimen number, S4410 (comparsion with clearance thickness, 2.0 mm and 0 mm between specimen and controller) there is no difference between the clearances. For the clearance, 1.0 mm, the second peak value decreases because a part folding is generated in the controller. Also, in the case of greater clearance between specimen and controller, a folding of specimen has been generated in the controller and those have caused the effects of regularly mode generation and at the same time, have brought torsion phenomena to members. Thus, it is thought that a clearance gap, 0.4 mm is appropriate between specimen and controller in the experimentation based on experimental process. As shown in Table 2 and Figure 10, C2 (h is 20 mm) specimen has the greatest absorbed energy in tests and the energy depends on the height of controller. Figure 14 shows a dynamic load-displacement diagram for the circular tube with the inner diameter, 39 mm and 10 mm in thickness. The second peak value is not observed unlike the static experimental results. Those phenomena were mostly observed within experimental ranges for the dynamic collapsed tests. Even if a crushing started at the 30°-machined trigger direction, the crushing could not be continued on the controller through a controller and once more the crushing had started at the opposite direction. It is thought that the controller restrained the progressive collapses due to the collapse phenomena for a short time (for example, about

Table 2. Energy absorption abilities under static loading.

Specimen No.	F_{max} [KN]	F_m [KN]	E_i [J]	E_t [J]
S3008CN	16.065	7.167	788.399	1433.453
S3008C102	14.058	6.655	732.055	1331.010
S3008C202	14.803	8.080	888.750	1615.910
S3008C302	16.063	7.263	798.936	1452.610
S3008C402	13.171	6.491	714	1298.182
S3010CN	18.519	8.840	972.345	1767.9
S3010C102	17.290	9.164	1008.041	1832.802
S3010C202	20.996	11.460	1260.581	2291.965
S3010C302	16.006	9.164	1008.041	1832.802
S3010C402	17.475	9.303	1023.330	1860.6
S3910CN	26.873	11.044	1214.791	2208.711
S3910C110	27.102	13.180	1449.816	2636.03
S3910C310	26.526	13.596	1495.599	2719.271
S3910C410	26.732	13.173	1449.014	2634.571
S3912CN	34.113	15.283	1681.106	3056.656
S3912C106	33.809	17.356	1909.105	3471.1
S3912C306	33.123	19.174	2109.181	3834.875
S3912C406	32.539	16.083	1769.140	3216.618
S4408CN	18.916	6.888	757.659	1377.562
S4408C100	19.673	7.652	841.724	1530.407
S4408C200	17.805	8.774	965.109	1754.744
S4408C300	20.311	7.750	852.531	1550.056
S4408C400	19.820	7.829	861.210	1565.836
S4410CN	27.441	11.191	1231.050	2238.273
S4410C120	26.757	12.650	1391.449	2529.907
S4410C320	27.006	12.488	1373.715	2497.664
S4410C420	27.798	12.042	1324.617	2408.395
S4410C100	28.209	12.327	1356.017	2465.485
S4410C200	29.031	14.047	1545.129	2809.325
S4410C300	27.319	12.232	1345.483	2446.333
S4410C400	28.089	11.634	1279.762	2326.840
S4412CN	33.893	16.151	1776.577	3230.140
S4412C116	34.115	16.6	1826.051	3320.093
S4412C316	34.341	18.259	2008.499	3651.816
S4412C416	34.437	17.073	1878.035	3414.609
S4412C100	34.983	16.373	1801.081	3274.693
S4412C200	33.495	17.857	1964.238	3571.342
S4412C300	33.269	15.867	1745.411	3173.475
S4412C400	32.997	16.191	1781.018	3238.215

200 ms). Also, when a table, impactor collides with a specimen, collapsing direction is horizontally kept between impactor and specimen to bring a collision without the deflection of specimens and clearance between a controller and specimens. Figure 15 shows relationship between

Table 3. Energy absorption abilities under dynamic loading.

Specimen No.	Input F_{max} [KN]	Input F_m [KN]	Input E_a [J]	Input E_t [J]	S [mm]
D3008CN	24.984	8.609	1062.376	1721.841	123.4
D3008c100	26.484	8.672	1051.896	1734.371	121.3
D3008C200	25.734	8.567	1016.457	1713.37	118.65
D3008C300	22.734	8.514	1089.754	1702.741	128
D3008C400	24.984	8.629	1078.619	1725.790	125
D3010CN	28.730	9.893	834.952	1978.559	84.4
D3010C100	30.982	11.863	886.791	2372.685	74.75
D3010C200	26.483	11.993	1014.650	2398.700	84.6
D3010C300	28.733	Buckling	Buckling	Buckling	151.7
D3010C400	28.732	11.880	996.743	2376.026	83.9
D3908CN	32.482	9.002	1093.707	1800.341	121.5
D3908C100	26.483	8.439	1110.536	1687.745	131.6
D3908C200	29.482	9.204	1064.899	1840.793	115.7
D3908C300	27.965	9.126	1158.997	1825.192	127
D3908C400	27.983	8.994	1077.494	1798.821	119.8
D3910CN	36.981	11.729	1148.258	2345.777	97.9
D3910C200	35.991	12.970	883.896	2593.972	68.15
D3910C300	36.984	15.681	952.619	3136.194	60.75
D4408CN	30.232	8.358	1032.991	1671.506	123.6
D4408C104	28.912	9.355	922.386	1870.966	98.6
D4408C204	30.232	9.187	893.864	1837.336	97.3
D4408C304	31.732	9.393	1122.919	1878.576	119.55
D4408C404	27.970	9.428	1109.694	1885.631	117.7
D4410CN	34.458	12.359	907.150	2471.798	73.4
D4410C100	34.120	11.314	939.048	2262.766	83
D4410C200	37.654	17.147	967.080	3429.362	56.4
D4410C300	36.259	11.524	940.325	2304.718	81.6
D4410C400	37.211	10.917	939.950	2183.391	86.1

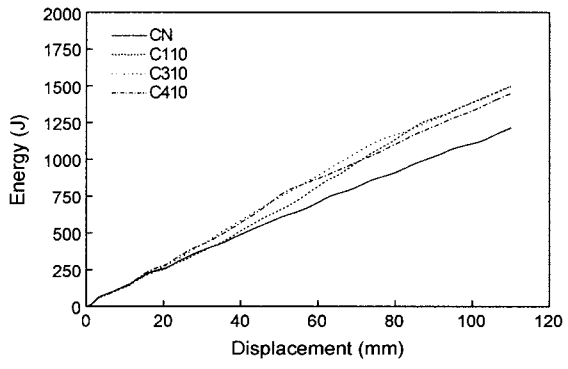

Figure 13. Static energy-displacement characteristics for the circular tube, S3910.

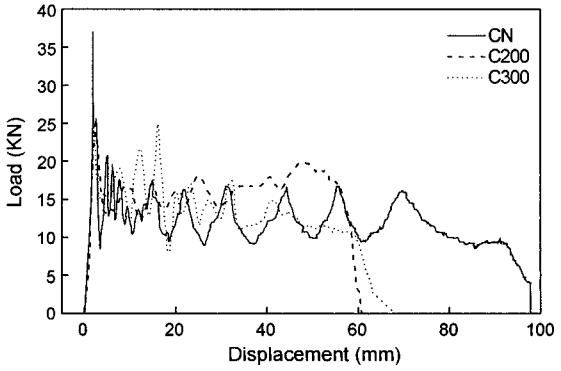

Figure 14. Dynamic load-displacement characteristics for the circular tube, D3910.

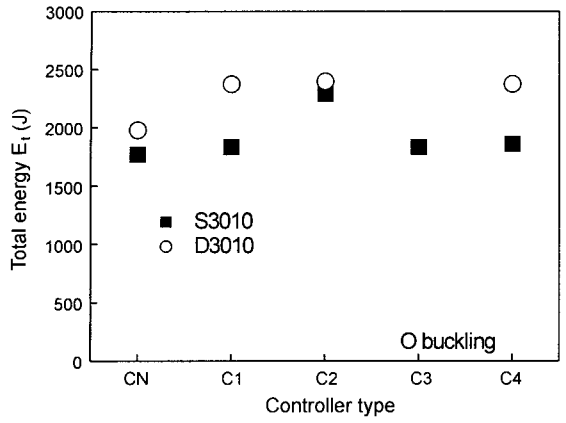

Figure 15. Relationship between controller type and total energy, 3010.

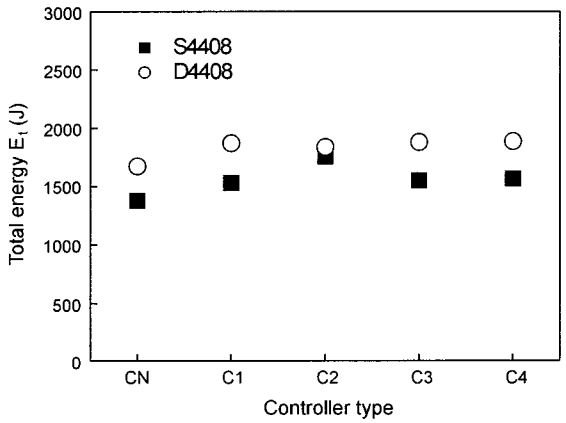

Figure 16. Relationship between controller type and total energy, 4408.

controller type and total energy for the circular tube with the inner diameter, 30 mm and 1.0 mm in thickness obtained from the static and dynamic collapsed experimentation. Total absorbed energy of C2 specimen becomes greater. Compared with CN specimen of static collapsed tests approximately 29.6% of C2 specimen is higher than that of CN specimen and approximately 21.2% of C2 specimen is greater than that of CN specimen. Also, in the case of dynamic collapse experimentation, the similar total absorbed energies of C1, C2, C4 and C4 specimens were absorbed on the controller generating foldings at the opposite direction without bringing the second folding. Figure 16 shows relationship between controller type and total absorbed energy for the circular tube with the inner diameter, 44 mm and 0.8 mm in thickness obtained from two static and dynamic collapsed experimentation. Those results are similar to those of Figure 15. From the results of Figure 16, total absorbed energies, 27.4% and 12.8% with using the controller are greater than those without

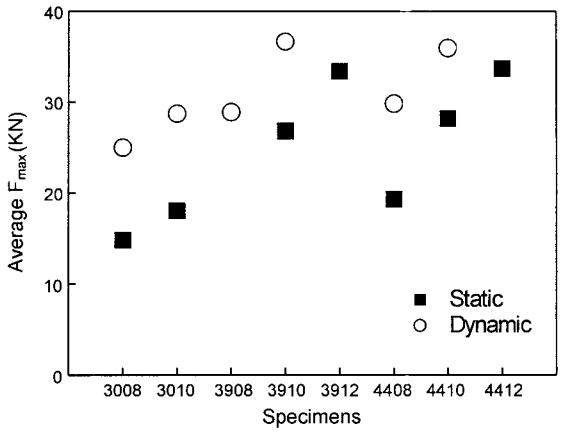

Figure 17. Relationship between specimens and average maximum load.

the controller, respectively. Also, in case of non-controller tests, the energy, 21.3% of dynamic collapsed test is greater than that of static collapsed test. Figure 17 shows relationship between specimens and average maximum load. The average maximum loads, 27.6% to 68.4% of dynamic collapsed tests are higher those of static collapsed tests. The thicker the specimen thickness, the greater the average maximum loading. Also, it is found that the average loadings are proportional to the dimension of cross area.

5. CONCLUSIONS

The horizontal impact testing machine was constructed to estimate the absorbed energy abilities with using a controller and a method to measure the load and the displacement diagram during crushing has been considered. The test tubes with the circular shapes are experimented under static and dynamic impact collapsed loading. The summary of the absorbed energy abilities of the thin-walled tubes under static and dynamic impact collapsed loading is as follows:

(1) There is no difference of energy absorption abilities even if thickness of a controller and clearance between specimen and controller are changed within the test range; however the more the height of controller, the greater the energy absorption abilities.

(2) Total absorption energies are increased to 10.6% ~29.6% and 12.8%~21.2% of the static and dynamic collapsed experimentation respectively by using a controller.

(3) 27.6%~68.4% of mean maximum collapsed loading in the dynamic collapsed test becomes higher than those of the loading in the static collapsed test and the thinner the thickness of specimen, the greater the difference of the collapsed loading.

(4) It is found out that the mixed modes with axisymmetric and non-axisymmetric crushing modes have been observed using the controller in this collapsed experimentation.

REFERENCES

Cha, C. S., Kang, J. Y., Kim, Y. N., Kim, J. H., Kim, S. K. and Yang, I. Y. (2001). Collapse characteristics on width ratio and flange spot-weld pitch for hat-shaped members. *KSME(A)*, **25**, **1**, 98–105.

Haug, E., Clinckemaillie, J., Ni, X., Pickett, A. K. and Queckborner, T. (1996). Recent trends and advances in crash simulation and design of vehicles. *Proceedings of the NATO-ASI*. July, 343–359.

Henry, J. C. Jr. (1995). A front rail design for efficient crush energy absorption. *Automotive Body Interior & Safety Systems IBEC'95*, 88–111.

Ishikawa, H. (1985). Computer simulation of automobile collision, reconstruction of accidents. *SAE Paper No. 851729.*

Kevin, J. (1986). *Air bag Technology Trends*, Automotive Engineering, 67–80.

Kim, S. K., Im, K. H., Yang, I. Y. and Adachi, T. (2001). Energy absorption control of vehicular-structure members. *Impact Engineering and Application.* **2**, 815–820.

Li, S. and Reid, S. R. (1990). Relationship between the elastic buckling of square tubes and rectangular plates. *International Journal of Applied Mechanics,* **57**, 969–973.

Mahmood, H. F. and Paluszny, A. (1981). Design of thin walled columns for crash energy management-their strength and mode of collapse. *Proc. 4rd International Conference on Vehicle Structural Mechanics*, Nov. 18–20, 7–18.

Singace, A. A. (1999). Axial crushing analysis of tubes deforming in the multi-lobe mode. *International Journal of Mechanical Science*, **41**, 865–890.

Pritz, H. B. (1983). Experimental investigation of pedestrian head impacts on hood and fenders of production vechicles. *SAE Paper No. 830055.*

White, M. D. and Jones, N. (1999). Experimental quasi-static axial crushing of top-hat and double-hat thin-walled sections. *International Journal of Mechanical Sciences*, **41**, 179–208.

White, M. D., Jones, N. and Abramowicz, W. (1999). A theoretical analysis for the quasi-static axial crushing of top-hat and double-hat thin-walled sections. *International Journal of Mechanical Sciences*, **41**, 209–233.

Wierzbicki, T. and Abramowicz, W. (1983). On the crushing mechanics of thin-walled structures. *J. Applied Mech.*, **50**, **4**, 727–734.